

Articulated Object Interaction in Unknown Scenes with Whole-Body Mobile Manipulation

Mayank Mittal^{†‡}, David Hoeller^{†*}, Farbod Farshidian[†], Marco Hutter[†], Animesh Garg^{‡*}

Abstract—A kitchen assistant needs to operate human-scale objects, such as cabinets and ovens, in unmapped environments with dynamic obstacles. Autonomous interactions in such real-world environments require integrating dexterous manipulation and fluid mobility. While mobile manipulators in different form-factors provide an extended workspace, their real-world adoption has been limited. This limitation is in part due to two main reasons: 1) inability to interact with unknown human-scale objects such as cabinets and ovens, and 2) inefficient coordination between the arm and the mobile base. Executing a high-level task for general objects requires a perceptual understanding of the object as well as adaptive whole-body control among dynamic obstacles. In this paper, we propose a two-stage architecture for autonomous interaction with large articulated objects in unknown environments. The first stage uses a learned model to estimate the articulated model of a target object from an RGB-D input and predicts an action-conditional sequence of states for interaction. The second stage comprises of a whole-body motion controller to manipulate the object along the generated kinematic plan. We show that our proposed pipeline can handle complicated static and dynamic kitchen settings. Moreover, we demonstrate that the proposed approach achieves better performance than commonly used control methods in mobile manipulation. For additional material, please check: www.pair.toronto.edu/articulated-mm/.

I. INTRODUCTION

The world we live in is full of objects designed by humans, for humans—our form and our abilities. For instance, our environments are rich in articulated objects, such as cabinets, drawers, and ovens. These objects contain multiple functional bodies that are kinematically linked to each other via mechanical joints. While operating in such environments, an agent would frequently need to interact with such objects. However, even everyday tasks, such as opening or closing a cabinet, impose fundamental challenges in interpreting the partially observable environment’s state and integrating that information to generate commands for safe execution.

Unlike in factories, where the environments can be designed to fit a robot’s needs and be modeled *a priori*, deploying autonomous service robots into human environments, such as households, is highly challenging [1]. There exist dramatic variations in these environments, such as in the rooms’ architecture or objects’ placement. Furthermore, even within an object category, there are differences between the object’s shape, size, and appearance. Thus, to interact successfully with a particular object instance, it is essential to reason over its properties. Additionally, to safely operate



Fig. 1: We present a generalizable mobile manipulation framework for articulated object interaction that can handle unknown spaces, variations within an object category, and dynamic scenes. Our method generates task-space plans through perception and ensures safe interaction through whole-body planning and online collision avoidance.

around other agents in the environment, real-time capabilities are necessary for handling dynamic changes.

Manipulation policies for articulated object interaction are obtainable through expert-defined strategies [2], [3] or are learnable from direct interactions or demonstrations [4]–[6]. However, the immense diversity of scenarios in human environments and limited interaction time available may lead to the failure of these approaches on new articulated objects [7]. Instead, estimating the articulation model through perception and incorporating that into planning [8], [9] allows better generalization and, thus, is a more promising approach.

Using a fixed-base manipulator for interacting with large articulated objects may not work due to its limited workspace. Developing autonomous robots for human environments depends on a seamless “integration of mobility and manipulation” [10]. To perform complex interactive tasks, it is essential to plan coordinated motions between the arm and the base together instead of separately. However, the complexity imposed by higher degrees of freedom (DOF) and the variety of constraints that need to be satisfied (such as joint limits, self-collision, and collision with the environment) make the motion generation a challenging problem.

In this paper, we propose a framework for mobile-based manipulation of articulated objects, which is composed of a two-level hierarchy— a *task scheduler* and a *primitive task tracker*. The task scheduler extracts the articulated properties of a targeted object using perceptual information. Knowing the object’s handle position, it generates task space keyframes for execution. The primitive task tracker, on the

[†] Robotic Systems Lab, ETH Zürich; [‡] University of Toronto, Vector Institute; * NVIDIA. Email: {mittalma, dhoeller, farshidian, mahutter}@ethz.ch, garg@cs.toronto.edu

other hand, comprises a whole-body motion controller, which follows the generated keyframe sequence to manipulate the object while satisfying various constraints and preventing collisions with the environment. While in this work, we make particular choices for each of the perception and control modules, their actual implementations are extendable by other model-based or data-driven solutions.

Our key contributions are as follows:

- 1) We present a perception-based mobile manipulation framework for performing articulated object manipulation, which generalizes to various object categories. To achieve this, we use data-driven canonical representation for articulated objects (Sec. IV).
- 2) Our proposed pipeline can handle complex kitchen settings, while ensuring safe navigation and manipulation through online collision avoidance (Sec. V).
- 3) We experimentally validate our framework in hyper-realistic simulation environments (Sec. VII). Compared to the commonly-used inverse kinematics-based method for planning, we show the proposed system improves the success rate by 134% and reduces the time taken by 26.5%. We also demonstrate our system's efficacy in handling dynamic obstacles.

II. RELATED WORK

Robotic manipulation of articulated objects has been researched for more than a decade. While an exhaustive survey is beyond the scope of this article, we mention a few recent efforts with respect to above listed contributions.

A. Learning Articulated Models

The task for inferring an object's kinematic structure has been addressed in various ways. In approaches based on interactive perception (IP), the robot actively interacts with the object, observes the changes, and uses it to estimate the articulation model [11]–[14]. However, these methods either rely on fiducial markers or require textured objects to observe the relative motion between the objects parts.

On the other hand, methods based on passive visual observations formulate the articulation parameters inference problem as a regression task [15]–[17] and leverage large synthetic datasets [18], [19]. Abbatematteo *et al.* [15] map a segmented depth image of an object into its kinematic model parameters and geometry by using mixture density networks. They assume that the kinematic graph structure of each object class is known *a priori*. Employing a similar assumption, Li *et al.* [16] leverage canonical representations to train a model for predicting part segmentation, part poses, and articulation parameters. Unlike these approaches, Jain *et al.* [17] perform category-independent articulation model estimation by creating a unified representation of different articulation models through screw theory. However, their method relies upon an input sequence of segmented depth images that show relative motion between two rigid parts of the object, which is hard to obtain in practice. In this work, we make use of articulation-aware canonical representations [16], as detailed in IV-A.

B. Motion Planning for Mobile Manipulators

To make the planning problem for mobile manipulators tractable, typically, the base navigation and arm manipulation planning are done separately [20]–[22]. An essential aspect of such a method is the robot base's positioning to maximize the arm's reachability. While inverse reachability maps (IRM) [23] help resolve this issue for the initial base placement, it does not consider the base movement during the object manipulation itself. To coordinate the base and arm during such interactions, recently, policies have been trained through reinforcement learning that either define sub-goals for the base and arm planners separately [4], [5] or generate kinematically feasible base movement commands [24].

Previous works on motion planning during articulated object manipulation [8], [9], [25] incorporate the object's kinematic model as a task space constraint and apply sampling-based planners with inverse kinematics (IK) to find feasible solutions. However, these methods are often computationally expensive, require offline planning, and may suffer from the shortcomings of IK when approaching singularities.

On the other hand, optimal control provides a framework to incorporate various constraints into the planner, perform real-time planning [26] and does not suffer from singularities [27]. Recent works on using this formulation for mobile manipulation have shown that a non-zero preview horizon in planning yields more robust and better solutions for operational space tracking [28], [29].

Pankert *et al.* [29] proposed a perceptive model predictive control (MPC) strategy that can track task-space trajectories while respecting the system's constraints, maintaining mechanical stability, and using visual information to avoid obstacles. In this work, we build upon this formulation to perform whole-body motion control during articulated object interaction, even during the presence of dynamic obstacles.

C. Holistic systems for articulated object interaction

Various systems combining navigation, grasping, articulation model estimation and motion planning have been proposed in the past [21], [22], [30]. Meeussen *et al.* [22] describe an integrated navigation system that performs vision and laser-based handle detection and opens doors using a compliant arm. They plan the base motion independently based on heuristics to prevent collisions with the door. Arduengo *et al.* [21] propose a system for door opening where they use a CNN-based detector for identifying door handles from RGB images and provide a probabilistic framework to infer a kinematic model from past experiences or human demonstrations. However, they blindly follow the generated task-space plan and do not consider online collision avoidance. Similarly, Rühr *et al.* [30] present a framework for operating unknown doors and drawers in kitchen spaces, which learns and stores articulation models in a semantic map for future retrieval. While they evaluate their method extensively in the real-world, the manipulation phase always start in front of the target object and it does not consider online collision avoidance as well.

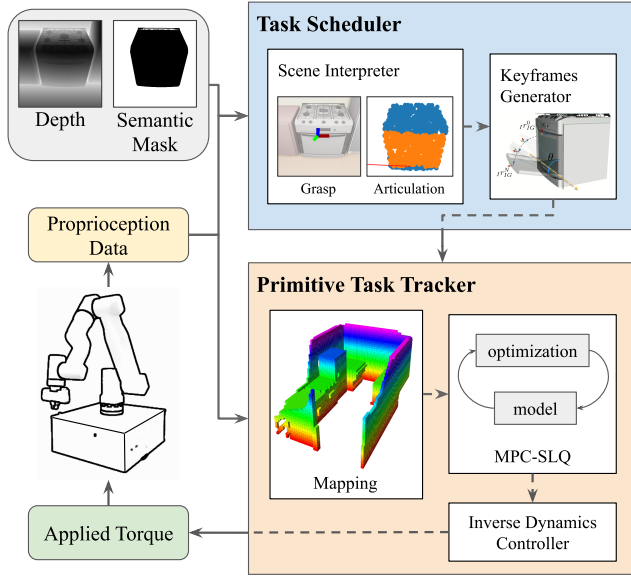


Fig. 2: The two-level hierarchy in the proposed framework. The task scheduler comprises a scene interpreter and keyframe generator, which uses perceptual information to generate task space plans for the robot. The primitive task tracker follows the generated plan while satisfying various constraints and performing online collision avoidance.

III. METHOD OVERVIEW

This work’s primary focus is performing perceptive-aware whole-body control for interacting with category-level novel articulated objects in unknown spaces. In this section, we first define the assumptions made in the proposed autonomy system and then describe its architecture, as shown in Fig. 2.

Building a complete autonomy system for articulated object interaction requires dealing with several challenges in machine perception, which are ongoing research topics in themselves. To this end, we assume that robot has access to following information: (i) semantic understanding of the scene for detecting and localizing the targeted object, (ii) location of the object’s handle for grasping, and (iii) a notion of ‘opening an object’ for conceptualizing task completion. Due to recent advances in computer vision, progress in semantic scene segmentation [31], [32] and grasp identification [21], [33] can be leveraged to lift some of these assumptions.

We propose a framework that comprises of a two-level hierarchy. The *task scheduler* acts as a scene interpreter and generates keyframes in the robot’s task space to interact with an articulated object. Using a depth image and a semantic mask of a targeted object, the scene interpreter estimates the object’s articulation properties. Once the articulation parameters are known, the keyframe generator computes a trajectory in the robot’s task space by evolving the estimated articulated object’s joint to its the desired state. Having obtained a reference task space trajectory, the *primitive task tracker* implements a motion control module to track this trajectory while ensuring constraints satisfaction and online collision avoidance using a signed distance fields (SDF) map.

It is important to note that the proposed structure is

highly modular. The components for scene interpretation and keyframes generation are replaceable by other data-driven and model-based solutions. Similarly, the motion control module’s formulation can utilize a robot’s kinematic or dynamic model, depending upon the robot and the task requirements. In this work, we describe one particular choice for the task scheduler and the primitive task tracker, as detailed in Sec. IV and Sec. V respectively, to show the designed system’s efficacy.

IV. TASK SCHEDULER

Articulated objects manipulation requires a detailed understanding of their articulation parameters (such as joint type, position, and axis orientation) and articulation state. Recently learning-based approaches have shown the possibility to learn representations directly from visual data [16], [17]. In this work, we utilize a similar approach based on [16] to estimate the object’s articulation parameters and its current state (Sec. IV-A). We then generate keyframes based on this description (Sec. IV-B).

A. Articulated Object Understanding Module

To extract the articulation properties, we use Articulation-aware Normalized Coordinate Space Hierarchy (ANCSH) representation [16], which is based on Normalized Object Coordinate Space (NOCS) [34]. In NOCS, the objects in a category are transformed into a 3D space such that they are zero-centered and uniformly scaled within a unit cube. ANCSH employs NOCS at two levels— one for the entire articulated object (NAOCS) and the other for its parts (NPCS). NAOCS provides the object-level reference frame where each joint is defined in its rest state. It looks at the parts from a holistic view and thus provides a consistent definition of joint parameters across various instances. On the other hand, NPCS is defined similarly to NOCS but for each individual part of the object. It provides a part reference frame and helps to define the pose and scale transform from NPCS to camera space. It is important to note that each NPCS can transform into its counterpart in NAOCS using scale and translation.

The network architecture for predicting the ANCSH representation is based on two PointNet++ modules [35]. It takes a point cloud as input, and its four heads output the part-wise segmentation, dense coordinates predictions in each NPCS, transformations from each NPCS to NAOCS, and the joint parameters in NAOCS. Using these predictions, pose-fitting is performed to robustly estimate the 6D pose and size of each part in the object. To avoid solutions where parts have physically impossible poses, the optimization scheme leverages kinematic constraints by adding an additional energy term based on the joint type. The resulting energy function is optimized by Umeyama algorithm [36] and non-linear least squares with RANSAC [37]. Once the poses of the objects have been estimated, the joint state and joint parameters can be computed in the camera space arithmetically. For further details about the pose optimization and training procedure, we refer the readers to [16].

B. Keyframe Generation

Once having an estimate of the object's current articulation parameters in the camera frame, we transform them to the world frame by using the camera pose. For a given grasp pose on the object's handle and the articulated object's desired state, we compute a discretized reference kinematic plan based on the joint articulation type and the object's current joint state. For a rotational joint, the kinematic plan is obtainable by rotating the grasp frame around the estimated joint axis [38]. In contrast, for a prismatic joint, the plan is obtainable through translation along the joint axis direction.

By simply reversing the keyframe plan obtained from above, we define a trajectory for approaching the object's handle. Once the robot's end-effector is close to the handle, the robot closes its gripper, and then, the kinematic plan for manipulating the object is used. The computed plans are followed by the primitive task tracker, as discussed below.

V. PRIMITIVE TASK TRACKER

In contrast to methods that consider separate, simplified models for base and arm motions, we formulate planning and control of mobile manipulation as a holistic optimization problem. The joint control of the base and the arm motion combined with a signed distance field representation of the environment enables our system to circumvent obstacles while performing a high-level task at the end-effector space. To solve this problem, we employ an MPC scheme where at each time step, t_s , the MPC solver receives a state measurement, \mathbf{x}_s and a local map of the environment. Based on these observations, MPC calculates the optimal control action sequence that drives the predicted system output to the desired reference. The robot's low-level control only executes the first piece of this optimized control sequence until the next MPC update arrives.

We consider the following nonlinear optimal control problem where the goal is to find the continuous control input in the time horizon $t_h = t_f - t_s$:

$$\underset{\mathbf{u}(\cdot)}{\text{minimize}} \quad \int_{t_s}^{t_f} l(\mathbf{x}(t), \mathbf{u}(t), t) dt, \quad (1a)$$

$$\text{subject to} \quad \mathbf{x}(t_s) = \mathbf{x}_s, \quad (1b)$$

$$\dot{\mathbf{x}} = \mathbf{f}(\mathbf{x}, \mathbf{u}, t), \quad (1c)$$

$$\mathbf{h}(\mathbf{x}, \mathbf{u}, t) \geq \mathbf{0}, \quad (1d)$$

where $\mathbf{x}(t)$ is the state and $\mathbf{u}(t)$ is the input at time t . l is a time-varying intermediate cost. The optimization is subjected to the initial condition (1b), system dynamics (1c), and general path constraints (1d).

Various methods exist to solve this problem [39], and a detailed discussion is beyond this paper's scope. In our implementation, we use the Sequential Linear Quadratic (SLQ) method [40], which is a continuous-time variant of the Differential Dynamic Programming (DDP) algorithm for systems with path constrained. The MPC problem is solved in a real-time fashion based on SLQ-MPC scheme [26].

We now briefly describe the main components of this MPC formulation: the system dynamic (Sec. V-A), the end-effector

tracking cost function (Sec. V-B), and collision avoidance constraints (Sec. V-C).

A. System Model

Our whole-body approach jointly plans for the base and the manipulator's motions. Generally speaking, there are two modeling approaches for such systems: a dynamic model [28] and a kinematic one [27]. Given our platform's specifications and the targeted tasks, we opt for the latter case. The robot in this work has a differential drive base with supporting passive castor wheels [29]. Thus, the base can turn in place but has a non-holonomic constraint and cannot drive sideways. The full base pose is defined in $SE(3)$ by its position $\mathbf{p}_{IB} \in \mathbb{R}^3$ and orientation $\mathbf{q}_{IB} \in SO(3)$ in the inertia frame. The system's state and input is defined as:

$$\mathbf{x} = (\mathbf{q}_{IB}, \mathbf{p}_{IB}, \mathbf{q}_j), \quad \mathbf{u} = (v_b, \omega_b, \mathbf{v}_j) \quad (2)$$

where v_b , ω_b are forward velocity and the turning rate of the base respectively, and \mathbf{q}_j , \mathbf{v}_j are the joint angles and velocities of the arm. These considerations lead to the following system model (1c):

$$\dot{\mathbf{x}} = \begin{bmatrix} \frac{1}{2} \mathbf{q}_{IB} \circ \omega_b \hat{\mathbf{k}} \\ \mathbf{q}_{IB} \circ v_b \hat{\mathbf{i}} \circ \bar{\mathbf{q}}_{IB} \\ \mathbf{v}_j \end{bmatrix} \quad (3)$$

with “ \circ ” denotes the quaternion product and $\hat{\mathbf{i}}, \hat{\mathbf{j}}, \hat{\mathbf{k}}$ the quaternion imaginary units. For a more detailed description of the robot's model, we refer the reader to [29].

B. Task Cost

We employ cost function for tasks defined in the robot's end-effector space. In general, the MPC formulation allows planning over pose, twist, and wrench of each end-effector. However, in this work, we only focus on the end-effector pose planning capability of our approach. Consequently, the task optimization variables per end-effector is in $SE(3)$ and the intermediate cost in problem (1) is written as:

$$l = \frac{1}{2} \|\mathbf{u}\|_{\mathbf{R}_u}^2 + \sum_i \|\mathbf{p}_{IE}^i - \tilde{\mathbf{p}}_{IE}^i\|_{\mathbf{Q}_p^i}^2 + \|\mathbf{e}_o^i\|_{\mathbf{Q}_o^i}^2, \quad (4)$$

where for the sake of brevity, the dependencies on state, input and time are dropped. The matrices \mathbf{Q}_p^i and \mathbf{Q}_o^i weights the position and orientation errors respectively at each end-effector and are positive semi-definite. The matrix \mathbf{R}_u penalizes high joint and base velocities and is a positive definite matrix. In Eq. (4), $\mathbf{p}_{IE}^i, \tilde{\mathbf{p}}_{IE}^i \in \mathbb{R}^3$ are the measured and desired positions of the i^{th} end-effector with respect to the inertial frame, I . We also define $\mathbf{e}_o^i \in \mathbb{R}^3$ to be an orientation error, which describes the deviation between a desired orientation and a measured one through the box minus operator.

C. System Constraints and Collision Avoidance

While tracking the end-effector, the generated motion plans should also respect various constraints such as joint limits of the arm, input limits and collisions. These are formulated into the MPC problem as follows:

1) *System Constraints*: Linear constraints, which restricts the joint positions of the arm and the velocity commands to the robot, are considered as a soft constraints, $\mathbf{z} := \mathbf{h}_{sys}(\mathbf{x}, \mathbf{u}, t) \geq \mathbf{0}$ and penalized through a relaxed logarithmic function defined as [41]:

$$B_{sys}(\mathbf{z}_j) = \begin{cases} -\mu \ln \mathbf{z}_j, & \mathbf{z}_j > \delta \\ \mu \beta(\mathbf{z}_j, \delta), & \mathbf{z}_j \leq \delta \end{cases} \quad (5)$$

where the function $\beta(\cdot, \cdot)$ is a quadratic function for which $B_{sys} \in \mathcal{C}^2$ and \mathbf{z}_j is the j^{th} system constraint. Following [29], we tune the hyperparameters $\mu = 5 \times 10^{-3}$ and $\delta = 10^{-4}$ for all the constraints.

2) *Collision Avoidance*: To prevent collisions with obstacles, we incorporate Euclidean signed distance field (ESDF) for defining a collision cost. The ESDF is generated online through the volumetric-mapping framework *FIESTA* [42]. The approach fuses depth images from the RGB-D camera into an occupancy map. From this map, the ESDF is derived using an efficient distance transform algorithm. We use trilinear interpolation to reduce the distance error induced by discretizing the grid map and compute the gradients using finite differences of the interpolated values.

To perform collision checking, we define a set of collision spheres to approximate the robot. The position of each collision sphere's center is computed using the forward kinematics of the robot. From each center, we query the cached distance and gradient information from the ESDF. Using this information, we write the collision constraint for the j^{th} collision sphere as:

$$h_j(\mathbf{x}, t) = \text{SDF}(\text{FK}_j^I(\mathbf{x}, t)) - r_j \geq 0, \quad (6)$$

where r_j is the radius of the sphere, $\text{FK}_j^I(\mathbf{x}, t)$ is the computed position of the sphere via forward kinematics and $\text{SDF}(\cdot)$ denotes the interpolated distance from ESDF.

Unlike [29], which uses an RBF function, we obtained better results by using a Squared-hinge function for the collision avoidance constraint $z_j := h_i(\mathbf{x}, t) \geq 0$:

$$H_j(z_j) = \begin{cases} 0, & z_j > \delta \\ \frac{\mu}{2}(z_j - \delta)^2, & z_j \leq \delta \end{cases} \quad (7)$$

We tune the hyperparameters $\mu = 5 \times 10^2$ and $\delta = 10^{-3}$.

VI. EXPERIMENTS

We evaluate our method extensively in high-fidelity kitchen environments created on NVIDIA Isaac Sim [43]. The simulator uses PhysX to provide stable, fast and realistic physics simulation while leveraging multi-GPU ray tracing to ensure photo-realism. In this section, we first summarize the simulation setup (Sec. VI-A) and describe the implementation specifics of our proposed pipeline (Sec. VI-B, Sec. VI-C). We then define the baselines and performance metrics for the evaluations (Sec. VI-D).

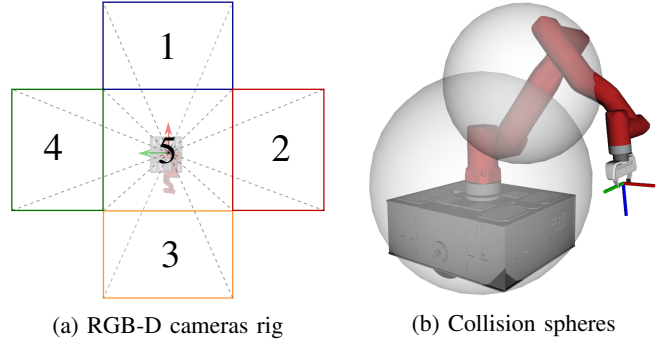


Fig. 3: Experimental setup for *MabiMobile* robot: (a) To provide 360° FoV, we mount five cameras on the robot base. (b) For collision checking, we coarsely approximate the robot with two collision spheres.

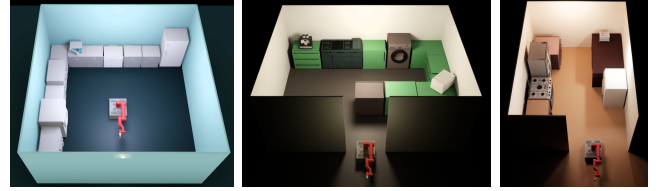


Fig. 4: Different kitchen scenes are designed in NVIDIA IsaacSim [43] using assets from the PartNet dataset [19]. The kitchens differ in architecture, the free space for mobility, and the articulated objects instances.

A. Simulation setup

1) *Robot platform*: For our experiments, we simulate the mobile manipulator *MabiMobile*. The robot has a differential drive base with four supporting castors, and a 6-DoF manipulator (*Mabi Speedy 12* by Mabi AG) mounted on it. We attached a parallel jaw gripper by Franka Emika on the robot arm to perform manipulation tasks.

For perception, we mount RGB-D cameras on the manipulator's shoulder such that the end-effector is visible during operation and around the robot base to ensure 360° Field-of-View (FoV), as shown in Fig. 3a. The cameras are simulated at a resolution of 512×512 pixels. We clip the ground-truth depth maps to 0.05m- 8.0m to match a typical depth sensor's range. The cameras on the base are used for online mapping; the points corresponding to the robot are filtering out using semantic masks.

2) *Kitchen environments*: We design three different kitchen layouts as shown in Fig. 4 using assets from PartNet dataset [19]. Each layout contains different instances of common objects found in modern kitchens, such as tables, refrigerators, and microwaves. Our experiments focus on three articulated object categories—ovens and washing machines (which have revolute joints) and cabinets (which have prismatic joints). We simulate the joints in these articulated instances as a spring-damped system which is randomized during the experiments.

B. Articulated Object Understanding Module

For estimating the articulation parameters of an object, we use the pre-trained networks provided by the authors of

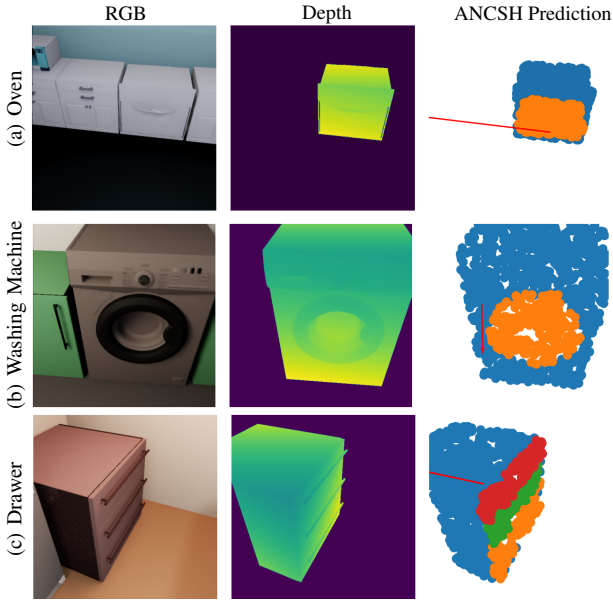


Fig. 5: Object’s articulation properties estimation using ANCSH [16]. Given a pointcloud of the target articulated object, ANCSH predicts its part-wise segmentation and joint properties. We visualize the results for particular instances of the three object categories considered in this work.

ANCSH. For the three categories considered in this work, the authors used CAD models from Shape2Motion [18] and PartNet [19] datasets to generate synthetic datasets from PyBullet rendering. We ensured that there is no overlap between the instances used by the authors for training and the test object instances in the designed kitchen environments for our experiments. Although the pre-trained networks for articulation model prediction were never trained with partially occluded pointcloud data, they generalize well to these cases, as shown qualitatively in Fig. 5.

C. Motion Planing and Control Module

We implement the control module using OCS2 toolbox¹. In all our experiments, we fix the time horizon of the MPC to 4s and compute the optimal solution at 30Hz. Instead of using a separate tracking module that follows the optimal whole-body trajectories, we evaluate the affine optimal policies with the latest state information of the system and send the computed command to the motor controllers [26].

For volumetric 3D mapping, we use *FIESTA* [42] at a resolution of 0.1m. We define two collision spheres on the robot, as shown in Fig. 3b. Since we cache the distances and gradients while computing the ESDF, adding more collision spheres should not add tangible computational overhead.

D. Baseline and Performance Metrics

Our choice for the primitive task tracker, whole-body MPC (SLQ-WBC), coordinates the base and arm to follow a given task space kinematic plan. We compare this approach to commonly used methods in which the base navigation

¹OCS2 toolbox available at: <https://bitbucket.org/leggedrobotics/ocs2>

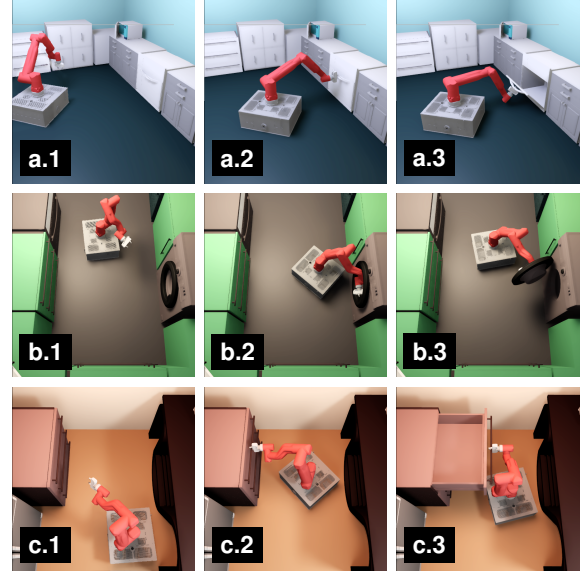


Fig. 6: The mobile manipulator in action for manipulation of different articulated objects in the three kitchens– (a) oven, (b) washing machine and (c) drawer. The spatial-awareness in the primitive task tracker ensures safe execution of the generated keyframes across diverse scenarios.

and object interaction are planned separately. To this end, we employ a sampling-based planning method, RRT* [44], to navigate the robot’s base in front of the target object. Subsequently, three different methods are used during the interaction: (i) arm-only control using MPC, (ii) whole-body planning using IK, and (iii) whole-body planning using MPC. We refer to these combinations as *RRT* + SLQ-Arm*, *RRT* + IK-WBC*, and *RRT* + SLQ-WBC* respectively.

For evaluating the performances of above motion controllers, we consider three metrics: (i) the percentage of evaluated runs that were successful, (ii) time taken to complete the task, and (iii) the path length travelled by the end-effector during successful executions. We say a given task is completed when the current joint position of the articulated object is more than a set threshold. For drawers, ovens and washing machines, these are defined at 65%, 60% and 75% of the articulated instance’s maximum joint limit.

VII. RESULTS

Fig. 6 provides illustrations of task execution using the proposed autonomy system for three object categories. In Fig. 7, we show the efficacy of the approach in online collision avoidance during interacting with the object. The motion controller tightly coordinates the base and arm to avoid the dynamic obstacle (which moves at 0.5 m s^{-1}) while ensuring tracking of the reference trajectory.

We evaluate the proposed pipeline in the three kitchen environments described in Sec. VI-A. For each articulated object category, we make 20 runs in each room while spawning the robot randomly into the scene. The averaged performance metrics are reported in Table I.

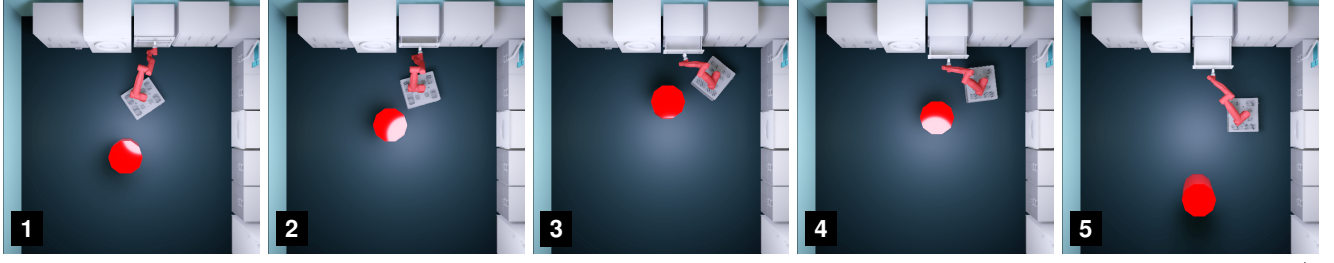


Fig. 7: The mobile-base manipulation of a drawer in a dynamic scene. The dynamic obstacle (which moves at 0.5 m/s). As the robot opens the articulated object, the control module ensures that generated kinematic plan from task scheduler is tracked while preventing collisions with the environment.

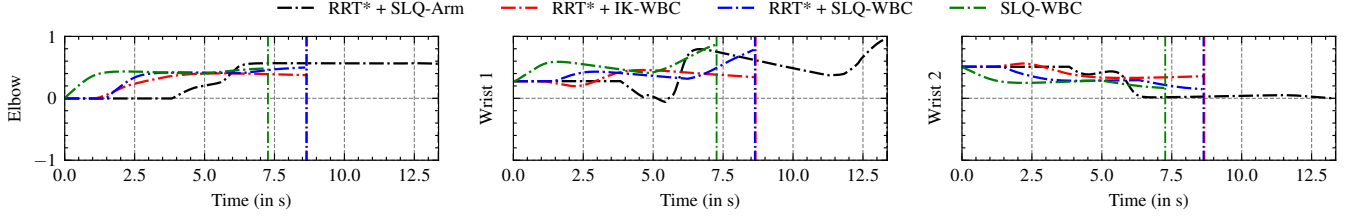


Fig. 8: State evolution for last three arm joints during oven manipulation. The joint states are normalized using their DoF limits. The colored vertical lines mark the end of the run, due to task completion, slippage, or hitting singularities.

TABLE I: Comparison of whole-body MPC (SLQ-WBC) against variants using RRT* for initial base navigation and a variant of the MPC for manipulation (SLQ-Arm, IK-WBC and SLQ-WBC). We report the results averaged from 60 runs. The time taken and end-effector (EE) path length are reported for trajectories corresponding to task completion.

Category	Algorithm	Success Rate (in %)	Time taken (in s)	EE Path length (in m)
Drawer	RRT* + SLQ-Arm	40.0	16.409 ± 3.353	7.761 ± 5.697
	RRT* + IK-WBC	55.0	17.843 ± 1.571	2.165 ± 0.378
	RRT* + SLQ-WBC	95.0	15.177 ± 0.729	5.011 ± 1.458
	SLQ-WBC	93.3	13.267 ± 0.651	3.711 ± 1.345
Oven	RRT* + SLQ-Arm	0.0	—	—
	RRT* + IK-WBC	20.0	11.523 ± 4.562	1.750 ± 0.175
	RRT* + SLQ-WBC	90.0	9.121 ± 0.659	3.090 ± 0.654
	SLQ-WBC	90.0	7.592 ± 0.459	2.638 ± 1.268
Washing Machine	RRT* + SLQ-Arm	0.0	—	—
	RRT* + IK-WBC	46.6	29.615 ± 5.202	4.243 ± 0.916
	RRT* + SLQ-WBC	96.6	22.952 ± 4.835	6.213 ± 4.071
	SLQ-WBC	95.0	18.747 ± 2.452	3.907 ± 0.739
Overall	RRT* + SLQ-Arm	13.3	19.475 ± 5.488	7.267 ± 4.831
	RRT* + IK-WBC	40.5	19.312 ± 6.752	3.854 ± 1.397
	RRT* + SLQ-WBC	93.8	15.616 ± 6.378	4.559 ± 2.855
	SLQ-WBC	92.7	14.152 ± 4.935	3.644 ± 1.301

The RRT* + SLQ-Arm baseline yields the most inferior performance across all three categories. In our experiments, we noticed that the baseline failed to track the kinematic plan for ovens and washing machines manipulation. This is due to the robotic arm reaching its joint limits during the interaction, as shown in Fig. 8.

The importance of a longer time horizon during planning is visible through the difference in the performance of RRT* + IK-WBC and RRT* + SLQ-WBC. By not having a look-ahead in IK-WBC, often the base is driven to a pose where it is hard to escape a collision with the environment². Compared to RRT* + IK-WBC, SLQ-WBC improves the overall success rate by 134% while reducing the average

time taken for task completion by 26.5%

Failure cases for the SLQ-MPC attribute to: (i) erroneous articulated properties estimation due to bad viewpoints (severe occlusions), and (ii) convergence to sub-optimal solutions where the gradient in favor of achieving the task competes with the one for preventing possible collisions.

By incorporating a global planner like RRT* to escape local optima, the RRT* + SLQ-WBC circumvents issue (ii); thus has a higher success rate than SLQ-WBC alone. However, since the RRT* + SLQ-WBC baseline first performs base navigation and then whole-body control for interaction, it is less efficient in executing the task than SLQ-WBC. A rather better approach to escaping local optima is utilizing the global plan to initialize the MPC solver.

²Videos available at: pair.toronto.edu/articulated-mm/.

VIII. CONCLUSION

We presented a two-stage hierarchy for autonomous mobile-based manipulation of articulated objects in unknown static and dynamic scenes. While the proposed paradigm is highly modular, we presented a particular set of choices for each of the stages and demonstrated the approach’s efficacy in diverse and complex kitchen settings. Through our experiments, we showed both qualitatively and quantitatively that the resulting autonomous system yields better performance compared to other commonly used control methods for mobile manipulation. In particular, our choice for the scene interpreter based on canonical representation (ANCSH) allows generalization across instances of a given articulated object category, even in the presence of occlusions. Moreover, our choice for the whole-body MPC controller (SLQ-WBC) allows the robot to safely track high-level end-effector references while ensuring a collision-free path during the interaction, even in the presence of dynamic obstacles.

In the future, we aim to improve further the system’s autonomy by leveraging data-driven or model-based approaches to alleviate some of the assumptions mentioned in Sec. III. These include grasp pose identification for the handle, using a dynamics model for the mobile manipulator, and performing hardware experiments.

REFERENCES

- [1] C. C. Kemp, A. Edsinger, and E. Torres-Jara, “Challenges for robot manipulation in human environments [grand challenges of robotics],” *IEEE Robotics Automation Magazine*, 2007.
- [2] L. Peterson, D. Austin, and D. Kragic, “High-level control of a mobile manipulator for door opening,” in *IROS*, 2000.
- [3] A. Jain and C. C. Kemp, “Pulling open novel doors and drawers with equilibrium point control,” in *ICHR*, 2009.
- [4] F. Xia, C. Li, R. Martín-Martín, O. Litany, A. Toshev, and S. Savarese, “Relmogen: Leveraging motion generation in reinforcement learning for mobile manipulation,” *arXiv preprint arXiv:2008.07792*, 2020.
- [5] C. Li, F. Xia, R. Martín-Martín, and S. Savarese, “Hrl4in: Hierarchical reinforcement learning for interactive navigation with mobile manipulators,” in *CoRL*, 2020.
- [6] T. Welschhold, C. Dornhege, and W. Burgard, “Learning mobile manipulation actions from human demonstrations,” in *IROS*, 2017.
- [7] O. Kroemer, S. Niekum, and G. Konidaris, “A review of robot learning for manipulation: Challenges, representations, and algorithms,” *JMLR*, 2021.
- [8] F. Burget, A. Hornung, and M. Bennewitz, “Whole-body motion planning for manipulation of articulated objects,” in *ICRA*, 2013.
- [9] S. Chitta, B. Cohen, and M. Likhachev, “Planning for autonomous door opening with a mobile manipulator,” in *ICRA*, 2010.
- [10] O. Khatib, K. Yokoi, O. Brock, K. Chang, and A. Casal, “Robots in Human Environments: Basic Autonomous Capabilities,” *IJRR*, 1999.
- [11] D. Katz and O. Brock, “Manipulating articulated objects with interactive perception,” in *ICRA*, 2008.
- [12] R. Martín-Martín, S. Hofer, and O. Brock, “An integrated approach to visual perception of articulated objects,” in *ICRA*, 2016.
- [13] J. Sturm, *Approaches to probabilistic model learning for mobile manipulation robots*. Springer, 2013.
- [14] K. Hausman, S. Niekum, S. Osentoski, and G. S. Sukhatme, “Active articulation model estimation through interactive perception,” in *ICRA*, 2015.
- [15] B. Abbatematteo, S. Tellex, and G. Konidaris, “Learning to generalize kinematic models to novel objects,” in *CoRL*, 2019.
- [16] X. Li, H. Wang, L. Yi, L. J. Guibas, A. L. Abbott, and S. Song, “Category-level articulated object pose estimation,” in *CVPR*, 2020.
- [17] A. Jain, R. Lioutikov, and S. Niekum, “Screwnet: Category-independent articulation model estimation from depth images using screw theory,” *arXiv preprint arXiv:2008.10518*, 2020.
- [18] X. Wang, B. Zhou, Y. Shi, X. Chen, Q. Zhao, and K. Xu, “Shape2motion: Joint analysis of motion parts and attributes from 3d shapes,” in *CVPR*, 2019.
- [19] K. Mo, S. Zhu, A. X. Chang, L. Yi, S. Tripathi, L. J. Guibas, and H. Su, “PartNet: A large-scale benchmark for fine-grained and hierarchical part-level 3D object understanding,” in *CVPR*, 2019.
- [20] R. Diankov, S. S. Srinivasa, D. Ferguson, and J. Kuffner, “Manipulation planning with caging grasps,” in *ICHR*, 2008.
- [21] M. Arduengo, C. Torras, and L. Sentis, “Robust and adaptive door operation with a mobile manipulator robot,” *arXiv preprint arXiv:1902.09051*, 2019.
- [22] W. Meeussen, M. Wise, S. Glaser, S. Chitta, C. McGann, P. Mihelich, E. Marder-Eppstein, M. Muja, V. Erubimov, T. Foote, J. Hsu, R. B. Rusu, B. Marthi, G. Bradski, K. Konolige, B. Gerkey, and E. Berger, “Autonomous door opening and plugging in with a personal robot,” in *ICRA*, 2010.
- [23] N. Vahrenkamp, T. Asfour, and R. Dillmann, “Robot placement based on reachability inversion,” in *ICRA*, 2013.
- [24] D. Honerkamp, T. Welschhold, and A. Valada, “Learning kinematic feasibility for mobile manipulation through deep reinforcement learning,” *arXiv preprint arXiv:2101.05325*, 2021.
- [25] F. Burget, M. Bennewitz, and W. Burgard, “Bi2rrt*: An efficient sampling-based path planning framework for task-constrained mobile manipulation,” in *IROS*, 2016.
- [26] F. Farshidian, E. Jelavic, A. Satapathy, M. Giffthaler, and J. Buchli, “Real-time motion planning of legged robots: A model predictive control approach,” in *ICHR*, 2017.
- [27] M. Giffthaler, F. Farshidian, T. Sandy, L. Stadelmann, and J. Buchli, “Efficient kinematic planning for mobile manipulators with non-holonomic constraints using optimal control,” in *ICRA*, 2017.
- [28] M. V. Minniti, F. Farshidian, R. Grandia, and M. Hutter, “Whole-Body MPC for a Dynamically Stable Mobile Manipulator,” *IEEE RA-L*, 2019.
- [29] J. Pankert and M. Hutter, “Perceptive model predictive control for continuous mobile manipulation,” *IEEE RA-L*, 2020.
- [30] T. Rühr, J. Sturm, D. Pangercic, M. Beetz, and D. Cremers, “A generalized framework for opening doors and drawers in kitchen environments,” in *ICRA*, 2012.
- [31] K. He, G. Gkioxari, P. Dollár, and R. Girshick, “Mask r-cnn,” in *ICCV*, 2017.
- [32] D. Seichter, M. Köhler, B. Lewandowski, T. Wengelfeld, and H.-M. Gross, “Efficient rgb-d semantic segmentation for indoor scene analysis,” *arXiv preprint arXiv:2011.06961*, 2020.
- [33] K. Mo, L. Guibas, M. Mukadam, A. Gupta, and S. Tulsiani, “Where2act: From pixels to actions for articulated 3d objects,” *arXiv preprint arXiv:2101.02692*, 2021.
- [34] H. Wang, S. Sridhar, J. Huang, J. Valentin, S. Song, and L. J. Guibas, “Normalized object coordinate space for category-level 6d object pose and size estimation,” in *CVPR*, 2019.
- [35] C. R. Qi, L. Yi, H. Su, and L. J. Guibas, “Pointnet++: Deep hierarchical feature learning on point sets in a metric space,” in *NeurIPS*, 2017.
- [36] S. Umeyama, “Least-squares estimation of transformation parameters between two point patterns,” *IEEE T-PAMI*, 1991.
- [37] M. A. Fischler and R. C. Bolles, “Random sample consensus: a paradigm for model fitting with applications to image analysis and automated cartography,” *Communications of the ACM*, 1981.
- [38] E. Kovács, “Rotation about an arbitrary axis and reflection through an arbitrary plane,” in *Annales Mathematicae et Informaticae*, 2012.
- [39] J. B. Rawlings, D. Q. Mayne, and M. Diehl, *Model predictive control: theory, computation, and design*. Nob Hill Publishing Madison, WI, 2017.
- [40] F. Farshidian, M. Neunert, A. W. Winkler, G. Rey, and J. Buchli, “An efficient optimal planning and control framework for quadrupedal locomotion,” in *ICRA*, 2017.
- [41] C. Feller and C. Ebenbauer, “Relaxed logarithmic barrier function based model predictive control of linear systems,” *IEEE T-AC*, 2016.
- [42] L. Han, F. Gao, B. Zhou, and S. Shen, “FIESTA: Fast Incremental Euclidean Distance Fields for Online Motion Planning of Aerial Robots,” in *IROS*, 2019.
- [43] NVIDIA, “Nvidia omniverse™ platform,” <https://developer.nvidia.com/nvidia-omniverse-platform>, accessed: 2020-11-25.
- [44] S. Karaman and E. Frazzoli, “Sampling-based algorithms for optimal motion planning,” *IJRR*, 2011.